Hindawi
Mathematical Problems in Engineering
Volume 2017, Article ID 3834170, 11 pages
https://doi.org/10.1155/2017/3834170

Research Article

Lattice Boltzmann Simulation of Natural Convection in an Annulus between a Hexagonal Cylinder and a Square Enclosure

L. El Moutaouakil, Z. Zrikem, and A. Abdelbaki

Faculty of Sciences Semlalia, Cadi Ayyad University, LMFE, BP 2390, 40000 Marrakech, Morocco

Correspondence should be addressed to Z. Zrikem; zrikem@uca.ac.ma

Received 1 February 2017; Accepted 6 April 2017; Published 18 June 2017

Academic Editor: Arturo Pagano

Laminar natural convection in a water filled square enclosure containing at its center a horizontal hexagonal cylinder is studied by the lattice Boltzmann method. The hexagonal cylinder is heated while the walls of the cavity are maintained at the same cold temperature. Two orientations are treated, corresponding to two opposite sides of the hexagonal cross-section which are horizontal (case I) or vertical (case II). For each case, the results are presented in terms of streamlines, isotherms, local and average convective heat transfers as a function of the dimensionless size of the hexagonal cylinder cross-section ($0.1 \leq B \leq 0.4$), and the Rayleigh number ($10^3 \leq \mathrm{Ra} \leq 10^6$).

1. Introduction

The numerical simulation of natural convection of various fluids in different geometries has become the most widely used approach because of its low cost and the accuracy of its predictions. This is justified by the availability of reliable mathematical models and robust numerical methods that predict the fluid flow and heat transfer characteristics in practically all situations encountered. The lattice Boltzmann method is relatively new compared to the classical approaches based on the Navier-Stokes equations. This technique has been used with a great success to simulate different physical behaviors of magnetohydrodynamic fluids [1, 2], inhomogeneous mediums [3, 4], phase change materials [5, 6], flows with chemical reactions [7], and porous media [8, 9].

The lattice Boltzmann method is easier to implement for the numerical simulation of laminar natural flows in the complex geometries. Thus, it has been successfully implemented to predict the flow structures and heat transfers in enclosures of different shapes [10–12]. But its performances are even more remarkable in the simulation of natural convection in the annulus between a rectangular enclosure and a cylinder of circular cross-section [13–20], square cross-section [21–23], or elliptical cross-section [24]. However, one finds in the literature many other numerical works that treated the natural convection in such geometries by using the Navier-Stokes equations [25–28]. Generally, the system is heated by the cylinder and cooled by the cavity walls which are maintained at the same temperature.

In these studies, the effects of the shape, size, and position of the heating body on the dynamic and thermal fields in the cavity are analyzed. Thus, Hussain and Hussein [27] studied the effect of the position of a circular cylinder inside a square enclosure. These authors have shown that the position of the horizontal cylinder has an influence on the convective heat transfer which is proportional to the Rayleigh number. Concerning the size effect, it has been studied by Moukalled and Acharya [25] which showed that the average heat transfer is proportional to the cross-section size of the cylinder placed in the center of the cavity. The simultaneous effects of the size and position of a circular cylinder inside a square cavity were analyzed by Ding et al. [13]. The results found indicate that these two parameters have a great influence on the dynamic and thermal fields in the annulus between the circular cross-section and the cavity walls. The effect of the cross-section geometry of the heating cylinder on natural convection within a square cavity is studied by Ravnik and Škerget [28]. These authors found that a cylinder of elliptical

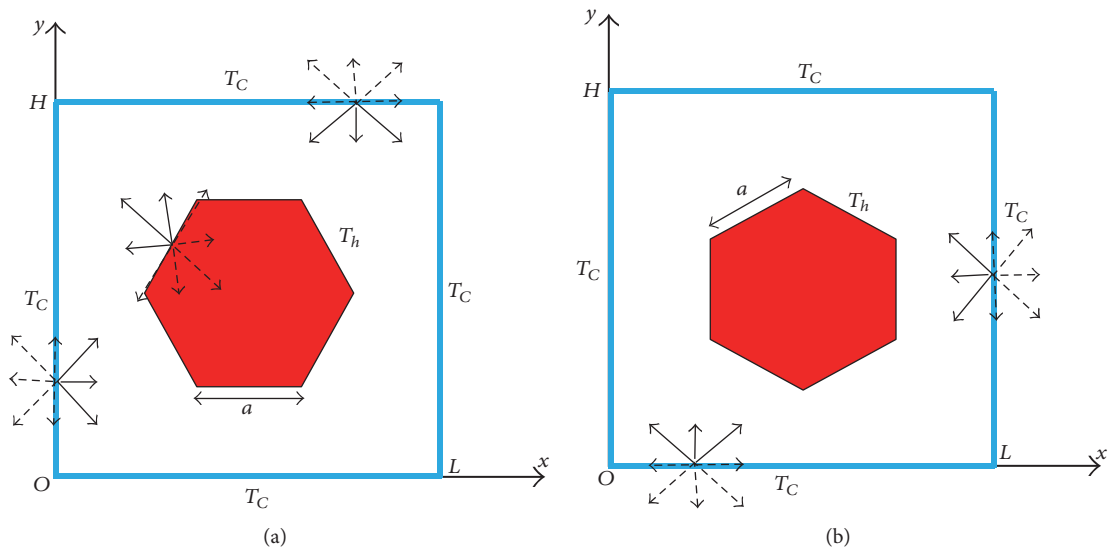

Figure 1: Studied configurations: (a) case I and (b) case II.

cross-section slightly improves the heat transfer through the walls of the cavity.

The literature review showed that the case of a horizontal hexagonal cylinder inserted in a square enclosure has not been studied. For this purpose, the present work is dedicated to the lattice Boltzmann simulation of two-dimensional natural convection around a horizontal hexagonal cylinder placed in a square cavity filled with water. The heating cylinder is at a hot temperature T_h, while the cavity walls are kept at a cold temperature T_C. The effects of the Rayleigh number, the size and orientation of the hexagonal cylinder on the streamlines, isotherms, and local and average heat transfers are presented and discussed below.

2. Mathematical Formulation

The system under consideration is a square cavity ($A = H/L = 1$), filled with water ($\mathrm{Pr} = 7$), and having four walls kept at a cold temperature T_C. A cylinder of hexagonal cross-section of side a is placed in the center of the cavity and maintained at a hot temperature T_h. The hexagon dimensions are such that $0.1 \leq B = a/L \leq 0.4$. Two orientations are considered, corresponding to two opposite sides of the hexagonal cross-section which are horizontal (case I) or vertical (case II) (Figure 1). The dimensions of the cavity and the temperature difference $(T_h - T_C)$ are varied so that $10^3 \leq \mathrm{Ra} = g\beta(T_h - T_C)L^3/\alpha\nu \leq 10^6$.

The thermophysical properties of water are considered constants, except the density in the buoyancy term where the Boussinesq approximation is adopted. To simulate the fluid flow and heat transfer in the physical domain, the lattice Boltzmann method (LBM) using the two distribution functions f and g, respectively, for the dynamic and thermal fields is implemented [29].

For the dynamic field:

$$f_i\left(\mathbf{r} + \mathbf{c_i}\Delta t, t + \Delta t\right) = f_i\left(\mathbf{r}, t\right) - \frac{1}{\tau_f}\left(f_i\left(\mathbf{r}, t\right) - f_i^{\mathrm{eq}}\left(\mathbf{r}, t\right)\right) + \Delta t F_i. \quad (1)$$

For the thermal field:

$$g_i\left(\mathbf{r} + \mathbf{c_i}\Delta t, t + \Delta t\right) = g_i\left(\mathbf{r}, t\right) - \frac{1}{\tau_g}\left(g_i\left(\mathbf{r}, t\right) - g_i^{\mathrm{eq}}\left(\mathbf{r}, t\right)\right). \quad (2)$$

The relaxation times for the flow and temperature fields are τ_f and τ_g, respectively. They are related to the kinematic viscosity and thermal diffusivity by

$$\nu = c_s^2\left(\tau_f - 0.5\right)\Delta t, \qquad \alpha = c_s^2\left(\tau_g - 0.5\right)\Delta t. \quad (3)$$

Note that the restriction $\tau > 0.5$ should be satisfied for both relaxation times to ensure that the kinematic viscosity and thermal diffusivity are positive.

The external force appearing in (1) is given by

$$F_i = \rho\omega_i\beta\frac{(T - T_C)}{c_s^2}\mathbf{g}\cdot\mathbf{c_i}. \quad (4)$$

Δt denotes the lattice time step. f_i^{eq} and g_i^{eq} are the equilibrium distribution functions which are calculated with the following relation:

$$f_i^{eq} = \rho\omega_i\left(1 + \frac{\mathbf{c_i}\cdot\mathbf{V}}{c_s^2} + \frac{(\mathbf{c_i}\cdot\mathbf{V})^2}{2c_s^4} - \frac{\mathbf{V}\cdot\mathbf{V}}{2c_s^2}\right)$$
$$\text{et } g_i^{eq} = T\omega_i\left(1 + \frac{\mathbf{c_i}\cdot\mathbf{V}}{c_s^2}\right). \quad (5)$$

c_s is the speed of sound. It is related to the velocity of the particles by

$$c_s = \frac{c}{\sqrt{3}}. \quad (6)$$

For both functions f and g, we adopt the D2Q9 model which contains nine propagation velocities of particles from a node $\mathbf{r}$ to its neighbors $\mathbf{r} + \mathbf{c_i}\Delta t$.

For the D2Q9 model, the weighting factor ω_i and the discrete velocities $\mathbf{c_i}$ are defined as follows:

$$\omega_i = \begin{cases} \frac{4}{9} & i = 1 \\ \frac{1}{9} & i = 2,3,4,5 \\ \frac{1}{36} & i = 6,7,8,9, \end{cases} \quad (7)$$

$$\mathbf{c_i} = \begin{cases} (0,0) & i = 1 \\ c\left(-\cos\left(\frac{i\pi}{2}\right), -\sin\left(\frac{i\pi}{2}\right)\right) & i = 2,3,4,5 \\ \sqrt{2}c\left(-\cos\left(\frac{[2i+1]\pi}{4}\right), -\sin\left(\frac{[2i+1]\pi}{4}\right)\right) & i = 6,7,8,9. \end{cases} \quad (8)$$

On the active walls, the boundary conditions for f_i and g_i are given by

$$f_i = f_j,$$
$$g_i = T_w\left(\omega_i + \omega_j\right) - g_j \quad (9)$$

with $T_w = T_h$ or T_C and $j = i + 2$ if $i = 2,3,6,7$ or $j = i - 2$ if $i = 4,5,8,9$.

The macroscopic quantities such as the density, velocity, and temperature are calculated by

$$\rho = \sum_{i=1}^{9} f_i,$$
$$\rho\mathbf{V} = \sum_{i=1}^{9} f_i\mathbf{c_i}, \quad (10)$$
$$T = \sum_{i=1}^{9} g_i.$$

Table 1: Validation in terms of Nu_C and ψ_{max} for different values of Ra and R.

(a) Nu_C

R/L	Ra	Moukalled and Acharya [25]	Ding et al. [13]	Present study
0.1	10^4	2.071	2.061	2.081
	10^5	3.825	3.752	3.750
	10^6	6.107	6.071	6.083
0.2	10^4	3.331	3.219	3.224
	10^5	5.080	4.896	4.874
	10^6	9.374	8.864	8.892
0.3	10^4	5.826	5.350	5.366
	10^5	6.212	6.202	6.186
	10^6	11.620	11.91	11.861

(b) ψ_{max}

	R/L	Moukalled and Acharya [25]			Present study		
		0.1	0.2	0.3	0.1	0.2	0.3
Ra	10^4	2.44	1.43	0.7	2.42	1.46	0.68
	10^5	14.3	11.8	7.19	14.42	11.93	7.22
	10^6	35.7	33.9	30	35.66	34.02	30.21

On a given cold wall, local and average Nusselt numbers are given, respectively, by

$$Nu_{CL} = \frac{\partial T}{\partial n},$$
$$Nu_C = \int_0^1 Nu_{CL}\,d\tau \quad (11)$$

on the horizontal walls $n = Y$ and $\tau = X$ and inversely on the vertical ones.

3. Numerical Procedure and Validation

In order to numerically integrate the equations (1) and (2), a computational mesh of 150 × 150 is used. In fact, it was found that the effect of a finer mesh on the results (Nu_C, ψ_{max}, and ψ_{min}) is negligible. The convergence is considered to be reached when the difference on the velocity and the temperature at each point of the mesh is less than 10^{-8} between two successive iterations.

For the computer code validation, the closest studies found in the literature are related to natural convection of air in an annulus between a cold square outer cylinder and a hot circular inner cylinder of radius R. The results of our code are compared in Tables 1(a) and 1(b) with those obtained by Moukalled and Acharya [25] and Ding et al. [13]. The good agreement on Nu_C (Table 1(a)) and ψ_{max} (Table 1(b)) may be noted for different values of Ra and R.

For Ra = 10^6 and $R/L = 0.1$, in Figure 2 the dimensionless velocity and temperature profiles at mid-height of the cavity are compared (between $X = 0.6$ and 1). The figure shows the excellent agreement on the velocity and

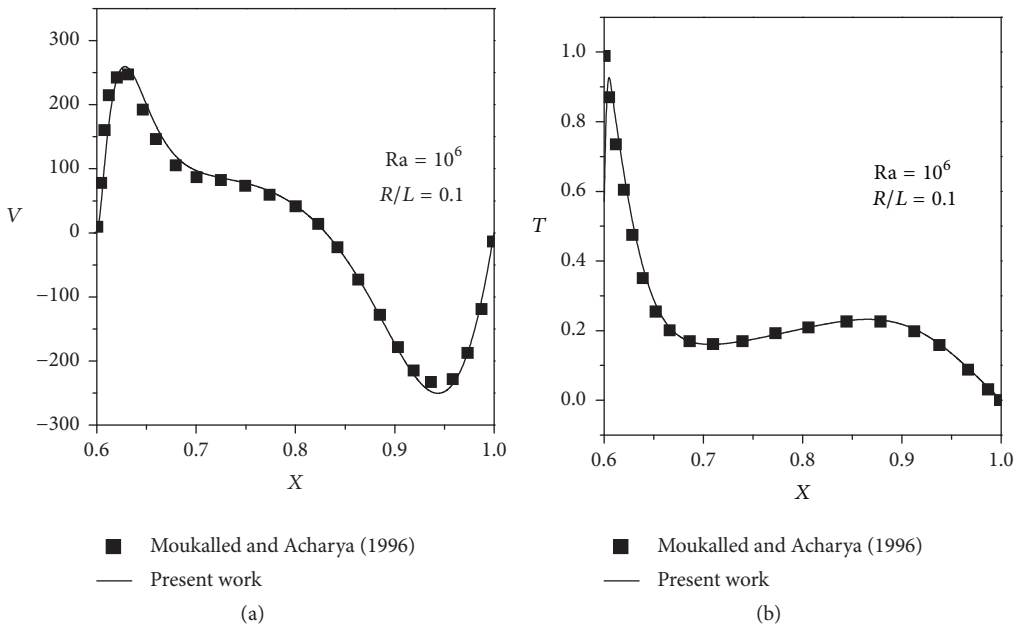

Figure 2: Validation for Ra = 10^6 and $R/L = 0.1$: (a) vertical velocity and (b) temperature.

temperature of the air (Pr = 0.71) that vary widely, especially near the hot circular wall.

4. Results and Discussion

4.1. Streamlines and Isotherms

4.1.1. Case I. For case I, Ra = 10^3 and different values of B (size of the heating body), the streamlines and isotherms are shown in Figures 3(a) and 3(b), respectively. Generally, the flow structures are symmetrical with respect to the center, the vertical and horizontal centerlines of the cavity. On either side of the vertical centerline, the convective cells have opposite rotations and their number increases with B, but their intensities decrease while remaining in general quite low. For $B = 0.4$, there are four cells that occupy the corners of the cavity. When B decreases, the size of these cells increases which allows those which rotate in the same sense to merge partially ($B = 0.2$) or totally ($B = 0.1$). Thus, for $B = 0.1$, we obtained only two separate cells that surround the cylinder and each of them occupies a vertical half of the cavity.

Due to the low intensity of the fluid flow (Ra = 10^3), the heat transfer between the cylinder and the cavity walls occurs mainly by conduction. Indeed, Figure 3(b) shows that, for a given B, the isotherms are almost symmetrical with respect to the vertical and horizontal median and indicate that the heat transfer is proportional to the hexagon size. For $B = 0.4$, the isotherms show a good heat transfer in the vicinities of the horizontal walls and the hexagon vertices that are near the vertical walls of the cavity, while for $B = 0.1$, the isotherms are almost circular with a spacing that increases with distance from the hexagon due to its small size.

Regardless of the size of the heated hexagonal cylinder, the fluid flow becomes much more intense for Ra = 10^6 and the symmetry with respect to the horizontal median is no longer observed (Figure 4(a)). Given that the temperature of the water is higher at the top of the cavity, the flow intensity is more important in this zone. For $B = 0.4$, we note the appearance of two small counter-rotating cells between the top horizontal walls of the hexagonal cylinder and the cavity. These convective cells are similar to those observed in the natural flows of Rayleigh-Bénard, while two large cells where each surrounds two small cells occupy the space between the cavity vertical walls and the hexagon. The intensity of the upper small cell is higher. For a small size of the hexagon, there are two large counter-rotating cells, each of which occupies a vertical part of the cavity, while in the vicinity of the bottom horizontal wall of the cavity, the fluid is stationary.

The isotherms of Figure 4(b) show that, regardless of the size of the heating body, the convective heat transfer is important over all sides of the hexagon and the top horizontal wall of the cavity. In addition, for $B = 0.4$, the isotherms show important thermal gradients in the whole domain including the bottom of the cavity. In contrast, for low values of B, the increase of the Rayleigh number promotes the thermal exchanges with the top horizontal cold wall and reduces them with the bottom one. Indeed, below the hexagon, the water temperature is practically uniform and equal to that of the cold walls. Note also the formation of a thermal plume when the size of the hexagon is small enough ($B = 0.2$ or 0.1).

4.1.2. Case II. For this new position of the hexagon (case II) and different values of B, the streamlines and isotherms are presented for Ra = 10^3 in Figures 5(a) and 5(b), respectively. Except for $B = 0.4$, the flow structures and their intensities have not undergone significant changes compared with case I. However, for $B = 0.4$, we have for this case only two large counter-rotating cells along the cold vertical walls, each of

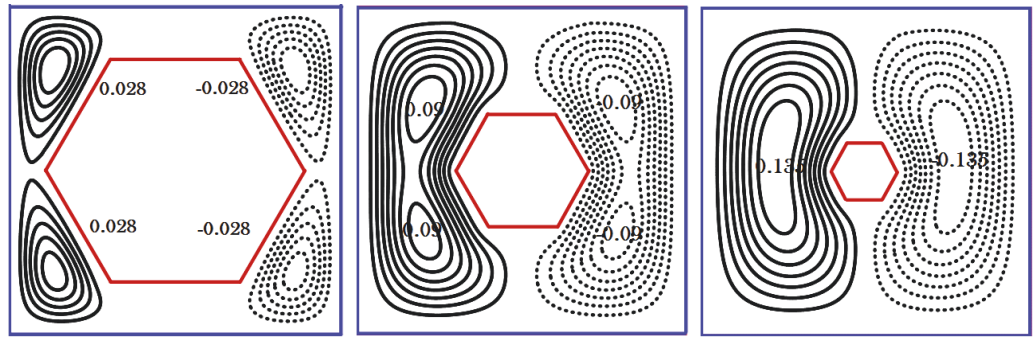

(a)

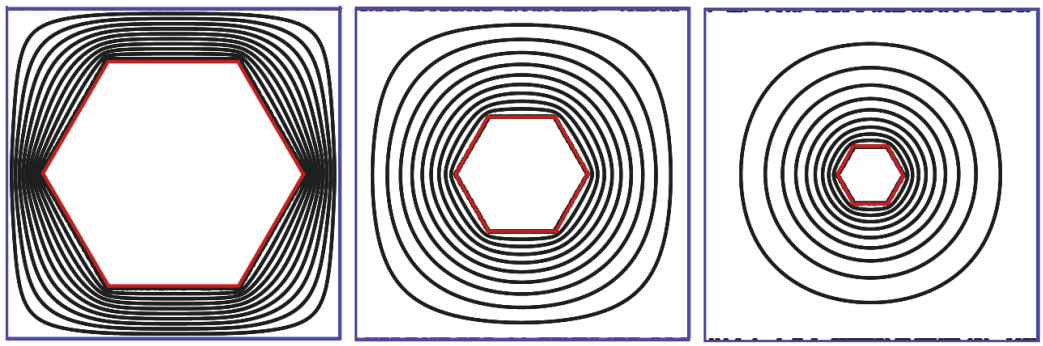

(b)

Figure 3: Contours for case I with Ra = 10^3 and B = 0.4, 0.2, and 0.1 (left to right): (a) streamlines and (b) isotherms.

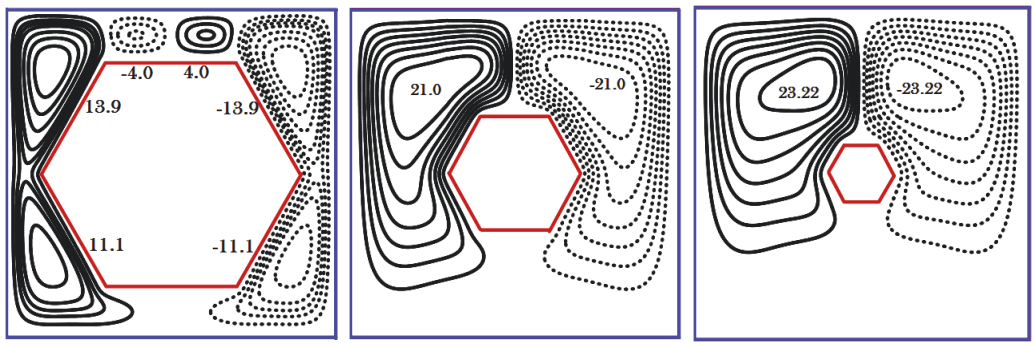

(a)

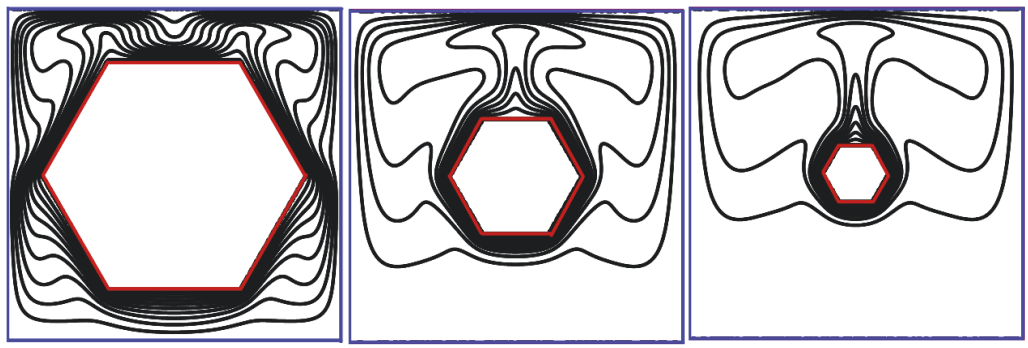

(b)

Figure 4: Contours for case I with Ra = 10^6 and B = 0.4, 0.2, and 0.1 (left to right): (a) streamlines and (b) isotherms.

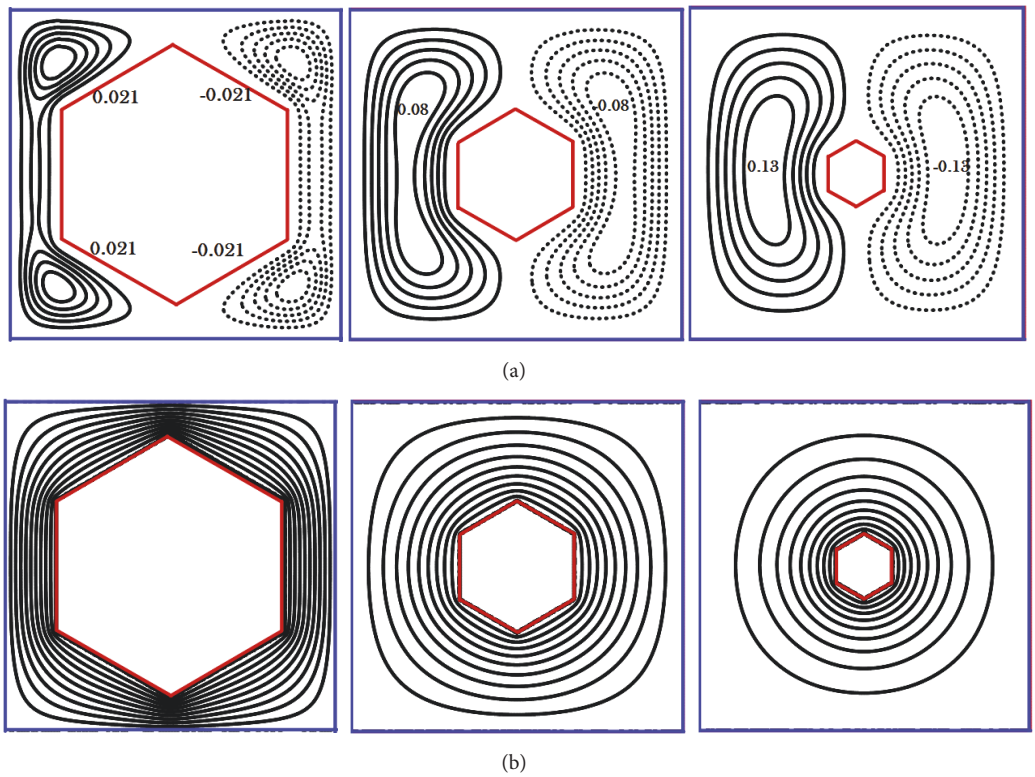

Figure 5: Contours for case II with Ra = 10^3 and B = 0.4, 0.2, and 0.1 (left to right): (a) streamlines and (b) isotherms.

which surrounds two small cells of a low intensity. As for the isotherms, they show also here that the heat transfer between the hexagonal cylinder and the walls of the cavity is mainly by conduction. The isotherms of case II can be deduced from those of case I by a simple rotation of 90° around the center of the cavity. Thus, for B = 0.4, the heat transfer is relatively better in the vicinity of the vertical cold walls and around the middle of the horizontal ones. While for B = 0.1 or 0.2, the isotherms remain circulars, so almost insensitive to the hexagon orientation.

By switching to Ra = 10^6 (Figures 6(a) and 6(b)), for low values of B, the influence of the orientation of the hexagon on the streamlines and isotherms is negligible. Only a slight effect on the thermal plume that is located over the top of the hot body is noticeable (Figures 4(a) and 4(b)). However, for B = 0.4, the dynamic and thermal fields have undergone significant changes relative to case I. Thus, the two small cells above the hexagon have undergone considerable reductions in size and intensity. While the most important changes are undergone by the isotherms, this will result in significant differences on local heat transfer along the cold walls of the cavity.

4.2. Heat Transfer. In conduction regime (Ra = 10^3), the variations of the local Nusselt numbers along the four cold walls of the cavity are presented in Figure 7 for the two cases and different values of B. Regardless of the value of B and the case considered, the evolution of Nu_{CL} on two opposite cold walls is almost identical and Nu_{CL} on the horizontal (vertical) wall of case II can be deduced from that on the vertical (horizontal) wall of case I.

For small sizes of the hexagon (B = 0.1 or 0.2), the variation of the local Nusselt number is generally independent of the cold wall considered and the orientation of the hot body (case I or II). The maximum and minimum values of Nu_{CL} are always obtained, respectively, at the middle (X = 0.5 or Y = 0.5) and the ends (X = 0 and 1 or Y = 0 and 1) of the considered wall. However, for B = 0.4, Nu_{CL} is highly dependent on the hexagon orientation in the cavity. Indeed, in case I, Nu_{CL} reached a maximum of 6.5 and 8.5 around the middle of the horizontal and vertical walls, respectively. While in case II, these same maximums of 6.5 and 8.5 are achieved around the middle of the vertical and horizontal walls, respectively.

For Ra = 10^6 and different values of B, the variations of Nu_{CL} on the horizontal and vertical cold walls are shown in Figures 8(a)–8(d). Firstly it is noted that the variation of Nu_{CL} on the top and bottom horizontal walls is no longer the same for all values of B. The hexagon orientation (case I or II) has virtually no influence on Nu_{CL} along all the cold walls when the hot body size is small enough (B = 0.1 and 0.2). $\mathrm{Nu}_{CL}(X)$ is proportional to B on the top cold wall and negligible on the bottom one. Due to the thermal plume shown by the isotherms (Figures 4 and 6), $\mathrm{Nu}_{CL}(X)$ is maximum at the middle of the top cold wall. However, the maximum value of $\mathrm{Nu}_{CL}(Y)$ is reached above the middle of the vertical walls. This behavior is caused by the progressive displacement of the cell centers to the top of the domain when Ra increases.

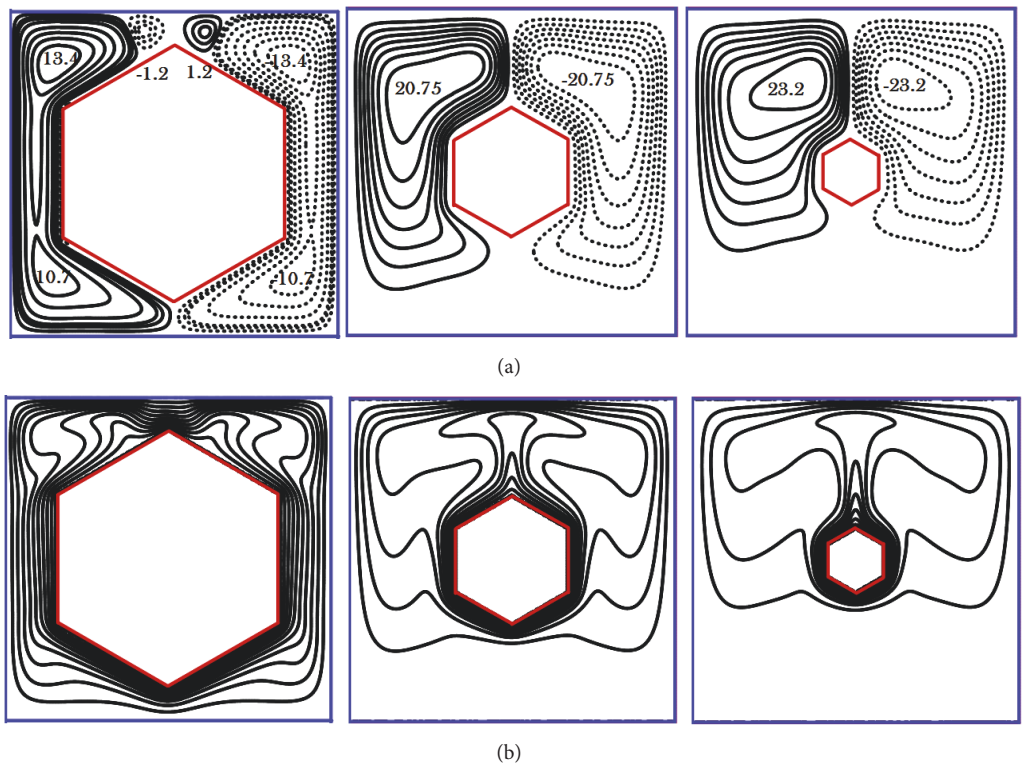

Figure 6: Contours for case II with Ra = 10^6 and B = 0.4, 0.2, and 0.1 (left to right): (a) streamlines and (b) isotherms.

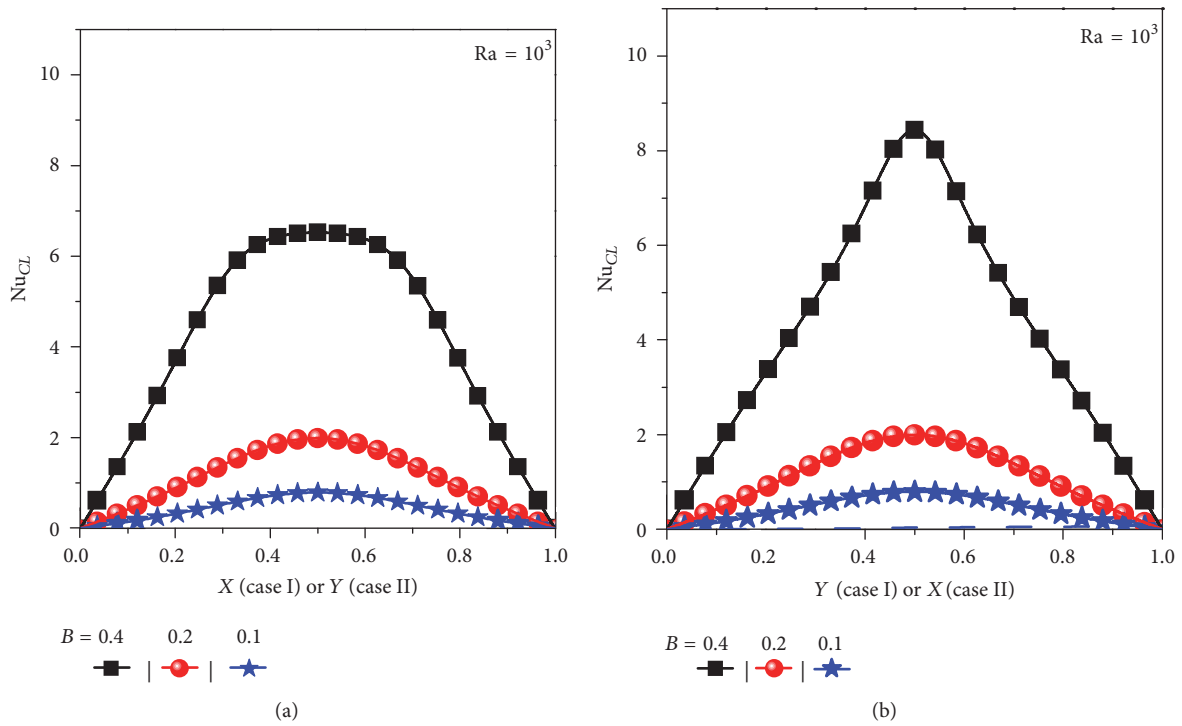

Figure 7: Variations of Nu_{CL} on cold walls for Ra = 10^3 and different values of B: (a) horizontal (case I) or vertical (case II) and (b) vertical (case I) or horizontal (case II).

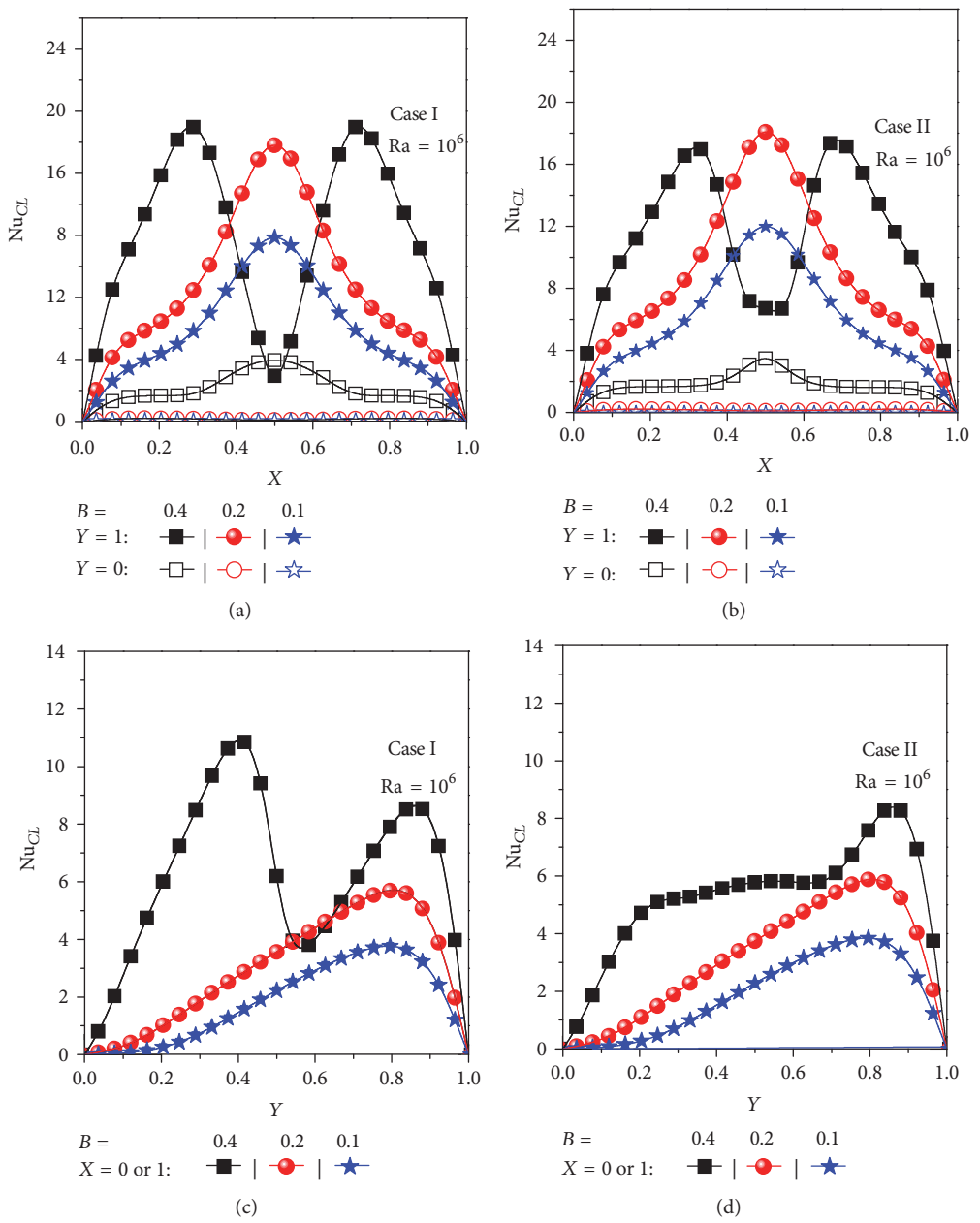

FIGURE 8: Variations of Nu_{CL} for Ra = 10^6 and different values of B: (a, b) horizontal walls and (c, d) vertical walls.

When the hexagon size is large ($B = 0.4$), its orientation has significant influence on the local heat transfer along the four walls of the cavity. For both cases, $Nu_{CL}(X)$ along the top horizontal wall is maximum at $X \sim 0.3$ and 0.7 ($Nu_{CL,max} \sim 18.5$ (case I) or 17 (case II)) and minimum at $X \sim 0.5$ ($Nu_{CL,min} \sim 3$ (cas I) or 6 (case II)). This behavior is due to the two small Rayleigh-Bénard cells that are formed at the top of the hexagon. Along the bottom cold wall, the heat transfer remains relatively low and $Nu_{CL}(X)$ reaches its maximum at $X \sim 0.5$. Concerning the two vertical walls, because of the symmetry, the variation of $Nu_{CL}(Y)$ is the same in each case. For case I, the fluid recirculation is reduced to the mid-height of the cavity, which gives a minimum local Nusselt number at $Y \sim 0.55$ with two peaks on either sides of this position. For case II, two sides of the hexagon are parallel to the vertical walls, resulting in a fairly regular local heat transfer around the middle of the walls. The maximum of $Nu_{CL}(Y)$ is located at the top where the intensity of the water flow is higher.

For both cases and different values of B, the average Nusselt numbers on all the cold walls of the cavity as a function of the Rayleigh number are presented in Figures 9(a)–9(c). For $B = 0.1$ and 0.2, Nu_C is independent of the hexagon orientation (case I or II) and it is always higher on the top horizontal wall. After a slight decrease between Ra = 10^3 and 10^4, Nu_C on the top horizontal wall increases rapidly

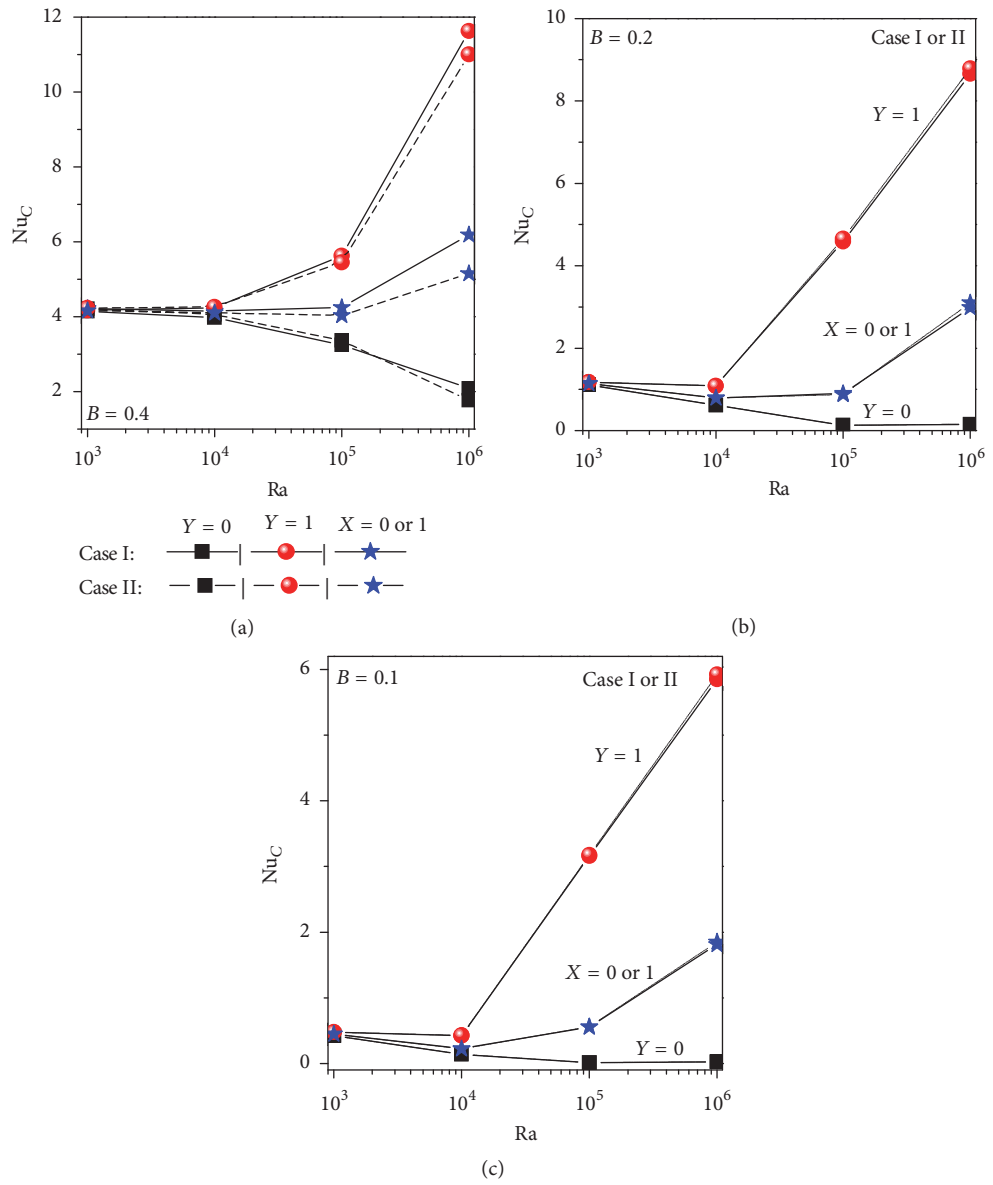

Figure 9: Average Nusselt numbers on the cold walls of cases I and II as a function of Ra: (a) $B = 0.4$, (b) $B = 0.2$, and (c) $B = 0.1$.

with Ra, while on the vertical walls, this growth is moderate. However, on the bottom horizontal wall, Nu_C is decreasing due to the displacement of the centers of the convective cells to the top of the cavity.

For $B = 0.4$, the proximity of the hot sides of the hexagon and the cold walls of the enclosure leads to higher convective heat exchanges. The orientation of the hexagon has an appreciable effect on Nu_C of all the cold walls, especially for high Rayleigh numbers. Overall, Nu_C is higher in case I and the difference with case II can reach about 20% on the vertical walls if $Ra = 10^6$.

5. Conclusion

The lattice Boltzmann method was used to study the natural convection of water around a hot horizontal hexagonal cylinder inserted in the center of a square enclosure with cold walls. For two orientations of the hexagon (cases I and II), the effects of the size B ($0.1 \leq B \leq 0.4$) and the Rayleigh number Ra ($10^3 \leq Ra \leq 10^6$) were studied.

For each case, it was found that the flow intensity and the number of convective cells depend on the size of the hexagon and the Rayleigh number. However, the effect of the orientation of the hexagon on the flow structures and heat transfers in the cavity is important only for high values of B. The average heat transfers through the walls of the cavity are proportional to B and are more favored in case I, if B and Ra are high.

Nomenclature

a: Side of the hexagon
B: Dimensionless size of the hexagon

$\mathbf{c_i}$: Discrete vector velocity
c_s: Sound speed
D2Q9: Lattice arrangement
$f_i(\mathbf{r}, t)$: Dynamical distribution function
$f_i^{\mathrm{eq}}(\mathbf{r}, t)$: Equilibrium dynamical distribution function
F_i: Directional imposed body force
$\mathbf{g}$: Acceleration due to gravity
$g_i(\mathbf{r}, t)$: Thermal distribution function
$g_i^{\mathrm{eq}}(\mathbf{r}, t)$: Equilibrium thermal distribution function
H: Cavity height
L: Cavity width
n: Normal
Nu: Nusselt number
Pr: Prandtl number
Ra: Rayleigh number
R: Radius
T: Dimensionless temperature
$\mathbf{V}$: Macroscopic vector velocity
X, Y: Dimensionless Cartesian coordinates.

Greek Letters

α: Thermal diffusivity
β: Thermal expansion coefficient
Δt: Time increment
ν: Kinetic viscosity
ρ: Fluid density
τ: Tangential
τ_f: Hydrodynamic relaxation parameter
τ_g: Thermal relaxation parameter
ψ: Stream function
ω_i: Weighting factor.

Subscripts

C: Convection, cold
h: Hot
i: Direction
L: Local
max: Maximum
min: Minimum
w: Wall.

Conflicts of Interest

The authors declare that they have no conflicts of interest.

References

[1] M. Sheikholeslami, M. G. Bandpy, and D. D. Ganji, "Lattice boltzmann method for MHD natural convection heat transfer using nanofluid," *Powder Technology*, vol. 254, pp. 82–93, 2014.

[2] M. Sheikholeslami, M. G. Bandpy, and K. Vajravelu, "Lattice Boltzmann simulation of magnetohydrodynamic natural convection heat transfer of Al_2O_3-water nanofluid in a horizontal cylindrical enclosure with an inner triangular cylinder," *International Journal of Heat and Mass Transfer*, vol. 80, pp. 16–25, 2015.

[3] P. R. Di Palma, C. Huber, and P. Viotti, "A new lattice Boltzmann model for interface reactions between immiscible fluids," *Advances in Water Resources*, vol. 82, pp. 139–149, 2015.

[4] L. Zhang and M. Wang, "Electro-osmosis in inhomogeneously charged microporous media by pore-scale modeling," *Journal of Colloid and Interface Science*, vol. 486, pp. 219–231, 2017.

[5] Y. Huo and Z. Rao, "Lattice Boltzmann simulation for solid-liquid phase change phenomenon of phase change material under constant heat flux," *International Journal of Heat and Mass Transfer*, vol. 86, pp. 197–206, 2015.

[6] K. Luo, F.-J. Yao, H.-L. Yi, and H.-P. Tan, "Lattice Boltzmann simulation of convection melting in complex heat storage systems filled with phase change materials," *Applied Thermal Engineering*, vol. 86, article 6579, pp. 238–250, 2015.

[7] C. S. Bresolin and A. A. M. Oliveira, "An algorithm based on collision theory for the lattice Boltzmann simulation of isothermal mass diffusion with chemical reaction," *Computer Physics Communications*, vol. 183, no. 12, pp. 2542–2549, 2012.

[8] Z. Chai, C. Huang, B. Shi, and Z. Guo, "A comparative study on the lattice Boltzmann models for predicting effective diffusivity of porous media," *International Journal of Heat and Mass Transfer*, vol. 98, pp. 687–696, 2016.

[9] M. Xia, "Pore-scale simulation of miscible displacement in porous media using the lattice Boltzmann method," *Computers and Geosciences*, vol. 88, pp. 30–40, 2016.

[10] M. Yousaf and S. Usman, "Effects of roughness elements on heat transfer during natural convection," *International Journal of Chemical, Molecular, Nuclear, Materials and Metallurgical Engineering*, vol. 9, pp. 1214–1219, 2015.

[11] B. Mliki, M. A. Abbassi, K. Guedri, and A. Omri, "Lattice Boltzmann simulation of natural convection in an L-Shaped enclosure in the presence of nanofluid, Engineering Science and Technology," *Engineering Science and Technology*, vol. 18, pp. 503–511.

[12] A. D'Orazio, A. Karimipour, A. H. Nezhad, and E. Shirani, "Lattice Boltzmann method with heat flux boundary condition applied to mixed convection in inclined lid driven cavity," *Meccanica. International Journal of Theoretical and Applied Mechanics*, vol. 50, no. 4, pp. 945–962, 2015.

[13] H. Ding, C. Shu, K. S. Heo, and Z. J. Lu, "Simulation of natural convection in eccentric annuli between a square outer cylinder and a circular inner cylinder using local MQ-DQ method," *Numerical Heat Transfer; Part A: Applications*, vol. 47, no. 3, pp. 291–313, 2005.

[14] K.-H. Lin, C.-C. Liao, S.-Y. Lien, and C.-A. Lin, "Thermal lattice Boltzmann simulations of natural convection with complex geometry," *Computers and Fluids*, vol. 35, pp. 35–44, 2012.

[15] Y. Hu, X.-D. Niu, S. Shu, H. Yuan, and M. Li, "Natural convection in a concentric annulus: a lattice boltzmann method study with boundary condition-enforced immersed boundary method," *Advances in Applied Mathematics and Mechanics*, vol. 5, no. 3, pp. 321–336, 2013.

[16] Y. Hu, D. Li, S. Shu, and X. Niu, "An efficient smoothed profile-lattice Boltzmann method for the simulation of forced and natural convection flows in complex geometries," *International Communications in Heat and Mass Transfer*, vol. 68, pp. 188–199, 2015.

[17] Y. Hu, D. Li, S. Shu, and X. Niu, "Study of multiple steady solutions for the 2D natural convection in a concentric horizontal annulus with a constant heat flux wall using immersed

boundary-lattice Boltzmann method," *International Journal of Heat and Mass Transfer*, vol. 81, pp. 591–601, 2015.

[18] Y. Hu, D. Li, S. Shu, and X. Niu, "Immersed boundary-lattice Boltzmann simulation of natural convection in a square enclosure with a cylinder covered by porous layer," *International Journal of Heat and Mass Transfer*, vol. 92, pp. 1166–1170, 2016.

[19] R. Khazaeli, S. Mortazavi, and M. Ashrafizaadeh, "Application of an immersed boundary treatment in simulation of natural convection problems with complex geometry via the lattice boltzmann method," *Journal of Applied Fluid Mechanics*, vol. 8, no. 2, pp. 309–321, 2015.

[20] M. Sheikholeslami, M. G. Bandpay, and D. D. Ganji, "Magnetic field effects on natural convection around a horizontal circular cylinder inside a square enclosure filled with nanofluid," *International Communications in Heat and Mass Transfer*, vol. 39, no. 7, pp. 978–986, 2012.

[21] M. Nazari, L. Loughalam, and M. H. Kayhani, "Lattice boltzmann simulation of double diffusive natural convection in a square cavity with a hot square obstacle," *Chinese Journal of Chemical Engineering*, vol. 23, pp. 22–30, 2014.

[22] A. K. Hussein, H. R. Ashorynejad, S. Sivasankaran, L. Kolsi, M. Shikholeslami, and I. K. Adegun, "Modeling of MHD natural convection in a square enclosure having an adiabatic square shaped body using Lattice Boltzmann Method," *Alexandria Engineering Journal*, vol. 55, no. 1, pp. 203–214, 2016.

[23] T. Zhang and D. Che, "Double MRT thermal lattice Boltzmann simulation for MHD natural convection of nanofluids in an inclined cavity with four square heat sources," *International Journal of Heat and Mass Transfer*, vol. 94, pp. 87–100, 2016.

[24] H. Bararnia, S. Soleimani, and D. D. Ganji, "Lattice Boltzmann simulation of natural convection around a horizontal elliptic cylinder inside a square enclosure," *International Communications in Heat and Mass Transfer*, vol. 38, no. 10, pp. 1436–1442, 2011.

[25] F. Moukalled and S. Acharya, "Natural convection in the annulus between concentric horizontal circular and square cylinders," *Journal of Thermophysics and Heat Transfer*, vol. 10, no. 3, pp. 524–531, 1996.

[26] S. M. A. Noori Rahim Abadi and A. Jafari, "Investigating the natural convection heat transfer from two elliptic cylinders in a closed cavity at different cylinder spacings," *Heat Transfer Research*, vol. 43, no. 3, pp. 259–284, 2012.

[27] S. H. Hussain and A. K. Hussein, "Numerical investigation of natural convection phenomena in a uniformly heated circular cylinder immersed in square enclosure filled with air at different vertical locations," *International Communications in Heat and Mass Transfer*, vol. 37, no. 8, pp. 1115–1126, 2010.

[28] J. Ravnik and L. Škerget, "A numerical study of nanofluid natural convection in a cubic enclosure with a circular and an ellipsoidal cylinder," *International Journal of Heat and Mass Transfer*, vol. 89, pp. 596–605, 2015.

[29] X. He, S. Chen, and G. D. Doolen, "A novel thermal model for the lattice Boltzmann method in incompressible limit," *Journal of Computational Physics*, vol. 146, no. 1, pp. 282–300, 1998.